IDENTIFICATION OF STRUCTURAL PROPERTIES OF THE INCIRLI PEDESTRIAN BRIDGE AND STRUCTURAL RESPONSE ANALYSIS

Nilgün Merve Çağlar[(1)], Erdal Şafak[(2)]

with Contributions from the HUB-Istanbul Researchers

[(1)] Boğaziçi University, Istanbul, Turkey, merve.caglar@boun.edu.tr

[(2)] Boğaziçi University , Istanbul, Turkey, erdal.safak@boun.edu.tr

TOMORROW'S CITIES TECHNICAL REPORT

February 2021

Tomorrow's Cities is the UKRI GCRF Urban Disaster Risk Hub

About Tomorrow's Cities

1.1.1 "Our mission is to reduce disaster risk for the poor in tomorrow's cities."

Tomorrow's Cities is the UK Research and Innovation (UKRI) Global Challenges Research Fund (GCRF) Urban Disaster Risk Hub – a five-year global interdisciplinary research hub.

Our aim is to catalyse a transition from crisis management to multi-hazard risk-informed and inclusive planning and decision-making, for cities in low-and-middle income countries.

Globally, more than two billion people living in cities of low-to-middle income countries are exposed to multiple hazards such as floods, earthquakes, landslides, volcanoes and fires, which threaten the cyclical destruction of their lives and livelihoods. With urban areas expanding at unprecedented rates, this number is expected to reach four billion by 2050.

Failure to integrate multi-hazard disaster risk into urban planning and decision-making presents a major barrier to sustainable development, including the single greatest global challenge of eradicating poverty in all its forms.

But this global challenge is also major opportunity: as ~60% of the area expected to be urban by 2030 remains to be built, we can reduce disaster risk in tomorrow's cities by design.

We are one of 12 UKRI GCRF Hubs funded by a UKRI Collective Fund Award, as part of the UK AID strategy, putting research at the heart of efforts to deliver the United Nation's Sustainable Development Goals (SDGs).

www.tomorrowscities.org
@UrbanRiskHub

The UKRI GCRF Urban Disaster Risk Hub

ECCI High School Yards, Infirmary Street, Edinburgh EH1 1LZ

Summary

Incirli Pedestrian bridge links the Bakirköy and Bahçelievler districts of Istanbul by crossing over the D100 highway and being exposed to heavy pedestrian traffic in peak-hours, since it is the only way to reach the Metrobus line for the people live in the neighboring area. The D100 is a state road with a total of 1852 km length, which extends from Kapıkule border crossing in Western Turkey to the Gürbulak border crossing point at Eastern Turkey. The highway has particular importance to Istanbul since it is one of the largest and busiest highways in the city. In the case of an emergency, D100 will be one of the most used alternatives to run efficient logistics operations in the city. Thus, studying the structural safety of pedestrian bridges over the D100 highway during earthquakes is very important, and this is the objective of this study.

Towards this objective, the seismic safety of one of such bridges, the Incirli pedestrian bridge, is studied by using vibration measurements, field inspections, a measurement-calibrated analytical model, and a site-specific design-spectra based analysis. The transfer matrix formulation is used to derive the properties of an equivalent SDOF structure. The elastic design spectra used is based on the latest Turkish seismic design code for the location, the TSC2018. Using the measured natural frequency of the structure and the elastic design spectra, the earthquake forces that are expected under several scenario earthquakes with different return periods are calculated, and the stress levels at the most critical sections of vertical structural elements are evaluated.

It is determined that, under the expected large Istanbul earthquake, the bridge is unsafe in its longitudinal direction, but safe in its transverse direction.

.

Acknowledgments

The authors are thankful to Emrullah Dar, Aslıhan Yolcu and Ahmet Korkmaz for providing their support in the field inspection and vibration measurements.

Table of Contents

List of Figures

List of Tables

2 Introduction

This report is prepared to present studies carried out to identify the seismic safety of the Incirli pedestrian bridge located in Bakirköy district of Istanbul.

This report starts with a brief description of the bridge and the fieldwork carried out to collect qualitative and quantitative data on the structure. It is then followed by the methodology for the analytical model and the analysis, and concludes with the results.

2.1 DESCRIPTION OF THE INCIRLI PEDESTRIAN BRIDGE AND THE FIELDWORK

Incirli Pedestrian bridge links the Bakirköy and Bahçelievler districts of Istanbul by crossing over the D100 highway and is exposed to heavy pedestrian traffic in peak commuting hours, since it is the only way to reach the Metrobus line for the people live in the neighboring area. The D100 is a state road with a total of 1852 km length, running from the Kapıkule border in the west to the Gürbulak border crossing in the east. The highway has particular importance to Istanbul, since it is one of the busiest highways in the city. In case of an emergency, D100 will be one of the most desired alternatives to run efficient logistical operations in the city. Thus, investigating the seismic safety of such pedestrian bridges over the D100 highway has a critical importance.

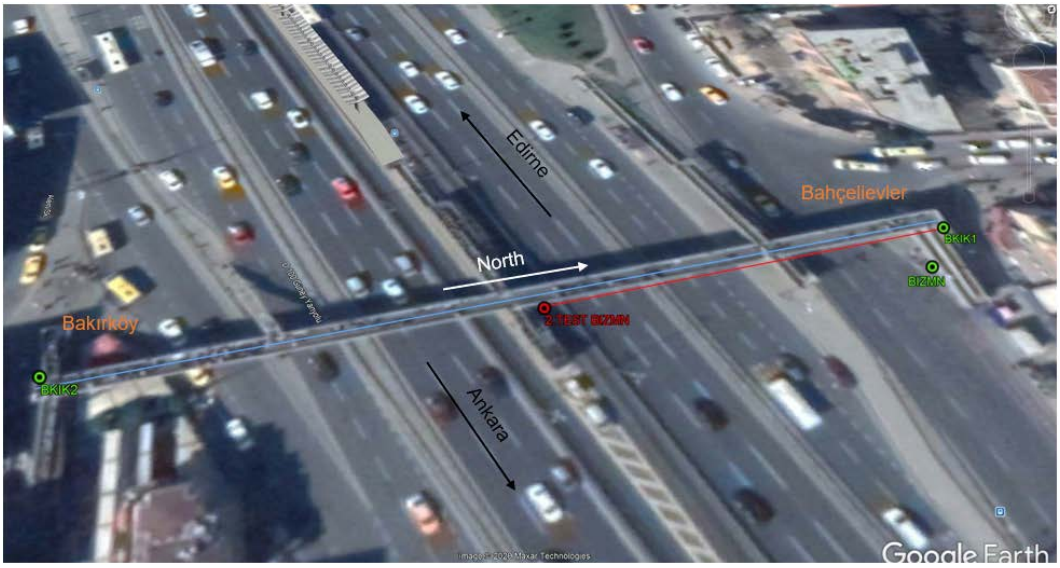

Fig. 2.1 Map showing the location of Incirli pedestrian bridge and installed sensors (Google Earth, 2021).

The structural model of the pedestrian bridge is constructed based upon the vibration measurements and the field inspection. Fig. 1.1 shows the location of both the Incirli pedestrian bridge and locations of acceleration sensors installed. The vibration measurements are conducted on March 12th, 2020 by using FBA (Force-Balance) type acceleration sensors. The first group of the recordings (Test1) corresponds to the time interval between 05:30 am

and 08:30 am. The sensor locations are marked by green dots in Fig. 1.1. The sensor **BIZMN** is located at the base level, and **BKIK1** and **BKIK2** sensors are located at the deck level. The second group of recordings (Test2) is collected between 08:51 am and 09:11 am. In Test2, the location of the **BIZMN** station is moved to the mid-point of the deck, as shown by a red dot in Fig. 1.1. The sampling rate of the accelerometers is 100 Hz.

The pedestrian bridge is made of structural steel and its total length is measured as ~115 m. The vertical elements of the bridge consist of 9 V-shaped columns with a height of ~5.7 m and span width of the deck segments vary from ~3 m. to ~27 m. The cross-sectional dimensions of the columns were measured at the point where they connected to the base and modeled as rectangular box sections in the analysis. The width of the deck is measured as ~2.9 m. The deck is supported by beams with a height of ~50 cm (measured from the edges of the deck). The transverse beams have a height of ~25 cm. Fig 1.2 shows the cross-section of the bridge in the North-South direction, the cross-section dimensions of the columns used in the analysis, and the profiles that form the deck.

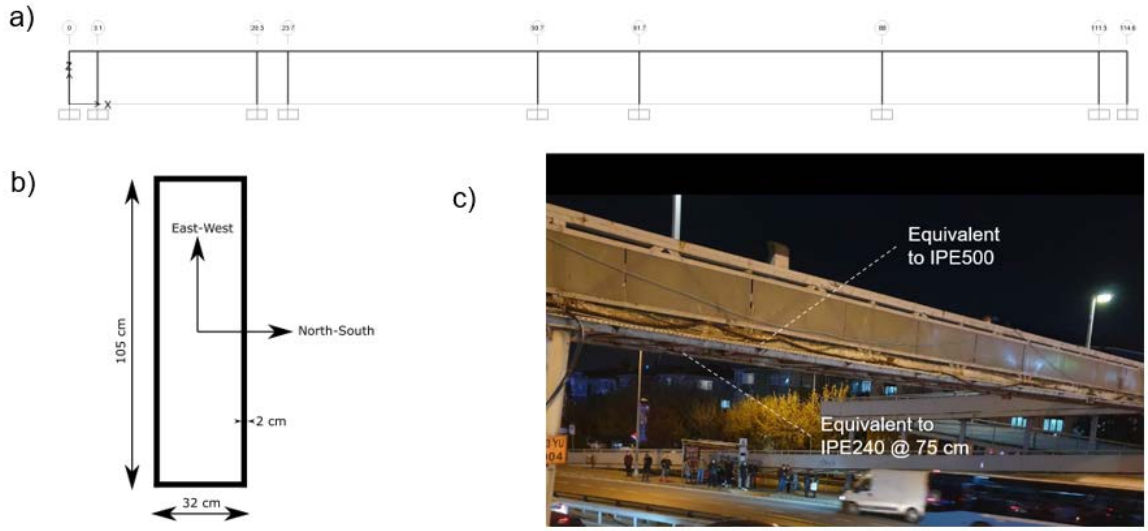

Fig. 2.2 a) Cross-section of the bridge in the North-South direction, b) the cross-section dimensions of the columns used in the analysis and c) the profiles that form the deck.

The information about the material quality is not available and it is estimated as S355 (TS EN 10025) type of steel, since it is the most common class used in pedestrian bridge construction in Turkey. The mass of the structure is estimated from the available data. The contribution of the stairs to the dynamic properties of the structure is neglected.

3 Analysis Methodology

In this section, we present the procedure for the analysis, which consists of four sequential steps. The analysis starts with the processing of the data from the vibration measurements, and identification of modal properties (i.e., frequency, damping, and mode shape) of the bridge. We then identify an equivalent a SDOF (Single Degree of Freedom) system for the bridge by using the transfer matrix formulation of dynamic response (Thomson, 1993).

The location-specific spectral acceleration levels suggested in the latest Turkish Seismic Design Code (TSC, 2018) for various return periods, and the identified dominant bridge frequency are used to calculate the forces. The base shear and the overturning moment are calculated and distributed over each structural component. Then, the stress level at each element due to bending moment and shear forces are determined.

3.1 DATA PROCESSING

The ambient vibration response of the structure is recorded using 3 triaxial (Guralp 5TDE; https://www.guralp.com/documents/DAS-050-0006.pdf) accelerometers, at 100 Hz sampling rate. Data processing included base-line corrections, band-pass filtering, and outlier removal (e.g., unintentional human contacts to the sensors during rush hours). We calculated the Cumulative Squared Acceleration (CSA) of the processed data to investigate the time variations of the bridge dynamic properties due to pedestrian traffic. The CSA is calculated in the time domain using Eq. (1) and gives a measure of the contribution to the root-mean-square (RMS) acceleration at each time step (Şafak et al., 1988).

$$U(t) = \frac{\int_0^t a^2(s)ds}{\int_0^{Tl} a^2(t)dt} \tag{1}$$

a(t) is the time history of the acceleration and Tl is the length of the record. Fig. 2.1 illustrates the CSA calculated at each time step of Test1 in each direction. As can be seen from the figure, the increase in the CSA at the beginning of the record (approximately the first 3600 s.) is much slower than the remaining part of the record.

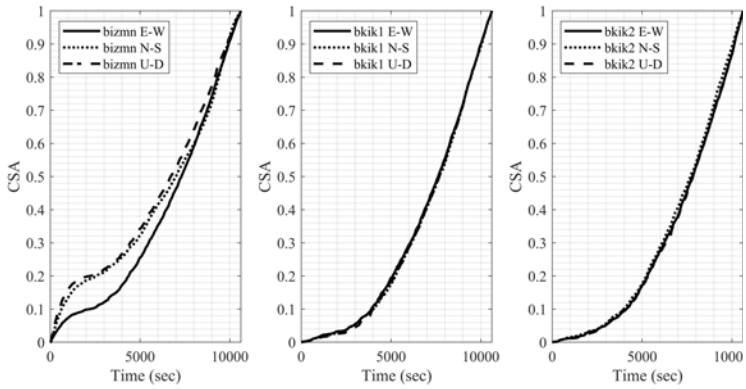

Fig. 3.1 Test1 CSA.

The abrupt change in the pattern of the CSA implies the increase in the pedestrian traffic over the bridge. Thus, the first and the second parts of Test1 records are processed separately. To exclude the part of recordings that contain environmental effects, the RMS amplitude is computed over a moving time window with 15 s of raw records. Time windows with RMS amplitudes within the 1 standard deviation of the mean are selected. Figs. 2.2 and 2.3 show the acceleration time series recorded during the first and second parts of Test1 (grey lines) and the selected time intervals (red lines) for analysis, respectively.

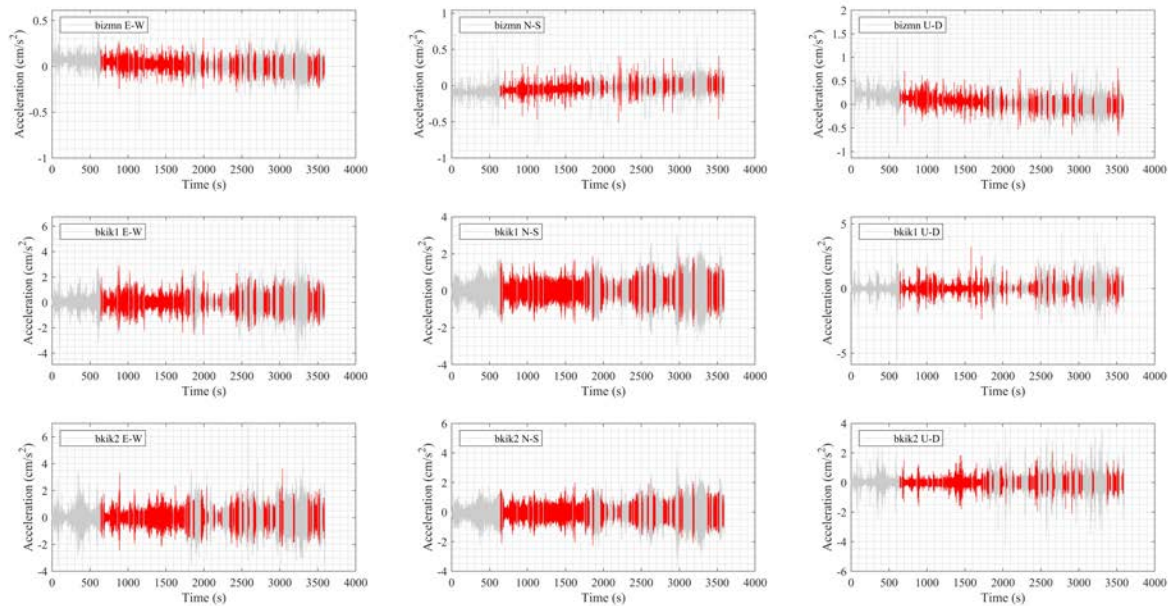

Fig. 3.2 Acceleration time series and the selected time windows corresponding to the first part of Test1.

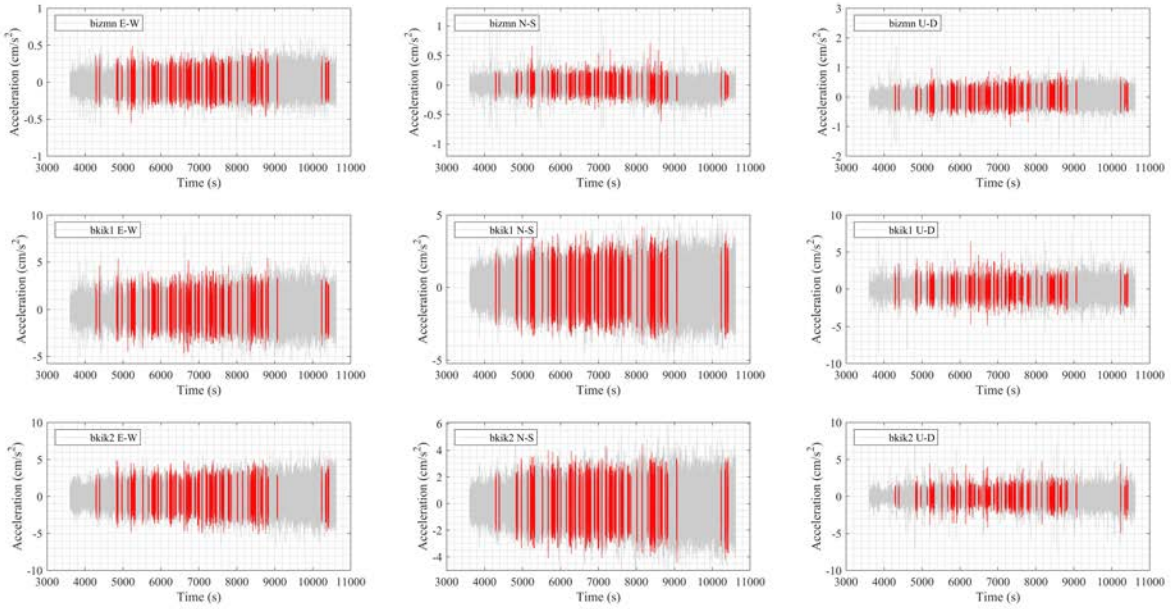

Fig. 3.3 Acceleration time series and the selected time windows corresponding to the second part of Test1.

The same procedure is applied to the Test2 record to extract time windows that will be used for identification. Fig. 2.4 shows the CSA calculated at each time step of Test2 in each direction. As can be seen from the figure the CSA increases linearly, which means that the contribution at each time step to the overall RMS acceleration is similar. Since these recordings belong to an ambient vibration of the structure, the CSA is expected to increase linearly.

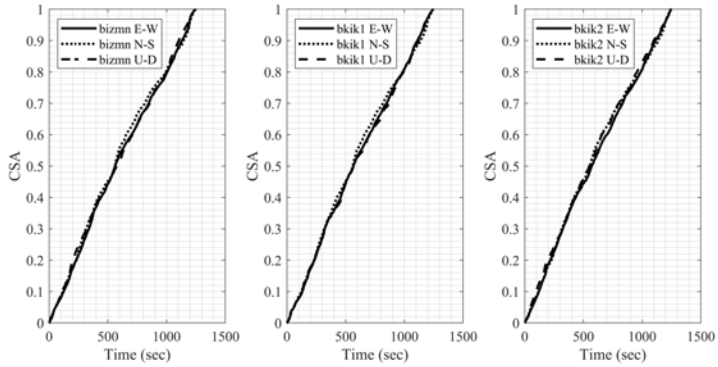

Fig. 3.4 Test2 CSA.

Fig. 2.5 shows the acceleration time series recorded during Test2 (grey lines) and selected time intervals from those recordings (red lines).

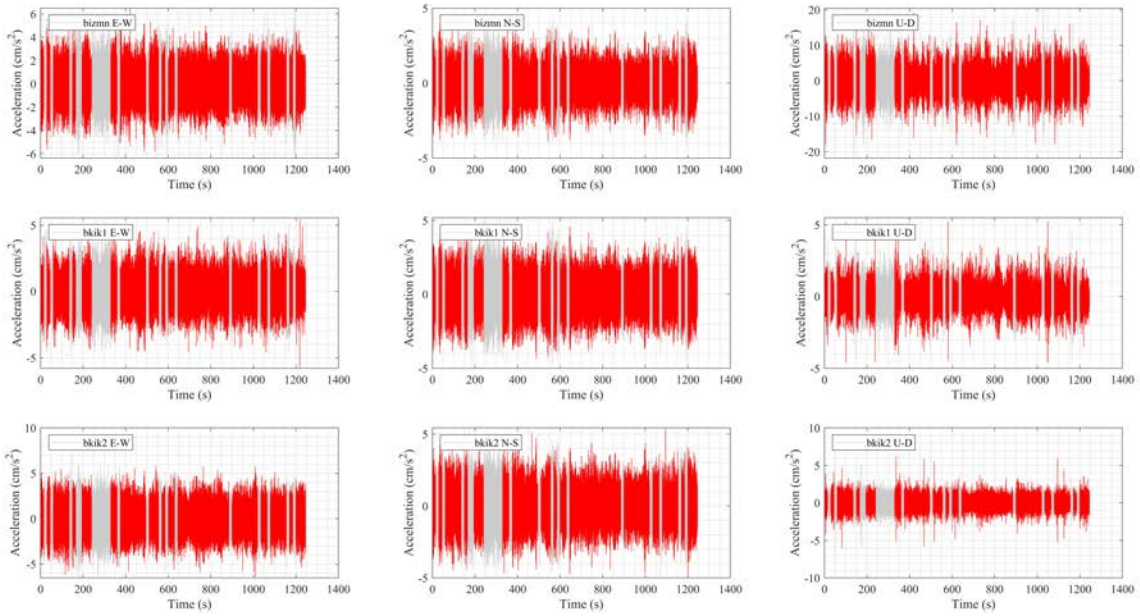

Fig. 3.5 Acceleration time series and the selected time windows corresponding to Test2.

A total of 103 and 92-time windows with 15 s. duration are selected from the first and second parts of Test1, respectively. 62-time windows with 15 s. duration are selected from Test2. Data in the selected time windows are band-pass filtered between 1-10 Hz, and used to identify the equivalent SDOF system for the bridge.

3.2 IDENTIFICATION OF DYNAMIC CHARACTERISTICS OF THE STRUCTURE

The properties of the equivalent SDOF of structure are estimated using the transfer matrix formulation of the response (Thomson, 1993). The methodology is also known as the Holzer's Method (Holzer, 1921) and it relates the dynamic response of two adjacent stations of a structure by providing the state vector for the force and displacement to be transferred from one station to the next (Kaya et al., 2015). Fig. 2.6 shows the forces and displacements acting on two adjacent stations considering shear forces only (Çetin, 2018).

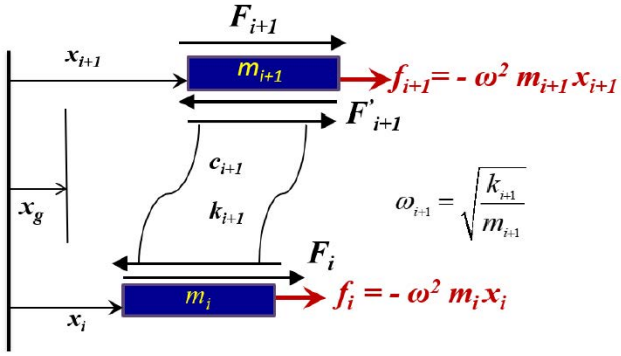

Fig. 3.6 Forces and displacements acting on two adjacent stations (Çetin, 2018).

In Fig. 2.6 the subscripts *i* and *i+1* denote the lower and upper stations, respectively. The parameters *x, m, f,* and *ω* denote the total displacement, mass, force, and radial frequency, respectively. The transfer matrix, which relates the accelerations and displacements of the upper floor to those of the lower floor is given by Eq. (2). The detailed derivation of the transfer matrix can be found in Kaya et al. (2015).

$$\begin{bmatrix} \ddot{X}_i(\omega) \\ F_i(\omega) \end{bmatrix} = \begin{bmatrix} 1 & -\omega^2/(k_{i+1} + i\omega c_{i+1}) \\ 0 & 1 \end{bmatrix}^{-1} \begin{bmatrix} 1 & 0 \\ -m_{i+1} & 1 \end{bmatrix} \begin{bmatrix} \ddot{X}_{i+1}(\omega) \\ F_{i+1}(\omega) \end{bmatrix} \tag{2}$$

The natural frequency corresponding to an equivalent SDOF system is estimated using an error minimizing algorithm, in which the calculated $\ddot{X}_i(\omega)$ is compared with the recorded one. The frequency that minimizes the error, Eq. (3), is the natural frequency of the equivalent SDOF system.

$$\varepsilon = \sum \left[\ddot{X}_i(\omega)_{recorded} - \ddot{X}_i(\omega)_{calculated} \right]^2 \tag{3}$$

As mentioned earlier, only the parts of the data that satisfy the RMS-based criterion are used in the procedure. The SDOF system that represents the dynamic characteristics of the structure in the N-S direction is derived using the **BKIK1-BIZMN** and **BKIK2-BIZMN** station pairs of the selected time windows of Test1 data. Similarly, properties of the SDOF system corresponding to the E-W direction is calculated using the E-W component of the same data.

Fig. 2.7 shows the natural frequency of the SDOF system corresponding to the N-S component of the response, calculated using time windows of the first part of Test1, **BKIK1** and **BIZMN** recordings, and the error term for the frequency band 1-10 Hz. As can be seen

from the figure, the natural frequency of the equivalent SDOF in the N-S direction varies between ~4.3 and ~4.7 Hz, and the mean of the data is 4.472 Hz.

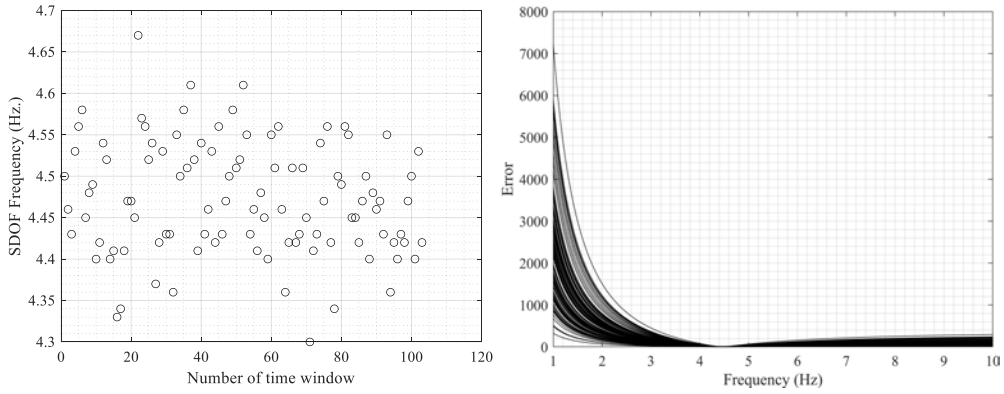

Fig. 3.7 Natural frequency of the equivalent SDOF system in the N-S direction using the first part of Test1 BKIK1 and BIZMN recordings and the calculated error term.

The natural frequency of the equivalent SDOF system for the N-S direction of the structure, and the error term corresponding to the frequency band 1-10 Hz are also calculated for same time windows of the first part of Test1, **BKIK2** and **BIZMN** recordings. As can be seen from Fig. 2.8, the natural frequency of the equivalent SDOF in the N-S direction varies between ~4.3 and ~4.7 Hz, and the mean of the data is 4.482 Hz.

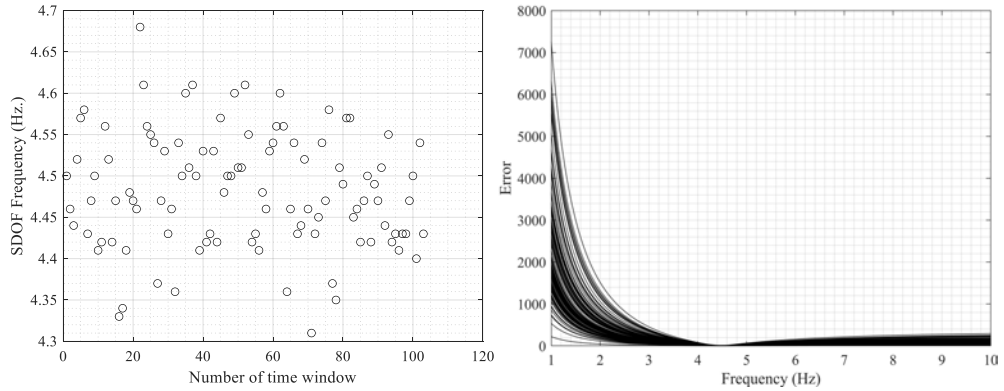

Fig. 3.8 Natural frequency of the equivalent SDOF system in the N-S direction using the first part of Test1 BKIK 2 and BIZMN recordings and the calculated error term.

Similar calculations using **BKIK1** and **BIZMN** recordings are performed for the second part of Test1 data, to estimate the properties of the SDOF system for the N-S and the E-W directions.

Table 1. The natural frequency of the equivalent SDOF in N-S and E-W directions.

	min	max	mean
2nd part Test1 N-S	4.32 Hz.	4.52 Hz.	4.424 Hz.
1st part Test1 E-W	6.32 Hz.	8.63 Hz.	7.72 Hz.
2nd part Test1 E-W	6. 56 Hz.	8.34 Hz.	7.391 Hz.

The up-down (U-D) components of recordings are used to calculate the pedestrian load effects on the mass. The total mass of the elements that form the deck is approximated as 100 t. The

natural frequency is calculated using the U-D components of **BKIK1** and **BKIK2** recordings for the first and second parts of Test1 and Test2 data.

Table 2. The natural frequency of the equivalent SDOF in the U-D direction

	min	max	mean
1st part Test1 U-D	1.90 Hz.	3.08 Hz.	2.655 Hz.
2nd part Test1 U-D	2.14 Hz.	2.99 Hz.	2.583 Hz.
2nd part Test2 U-D	2.13 Hz.	2.80 Hz.	2.573 Hz.

The difference between the natural frequencies obtained from the first part of Test1 and Test2 shows that the structure is exposed to approximately 5.6 ton increase in the total mass due to pedestrians.

3.3 CODE-SPECIFIED EARTHQUAKES

The 2018 Turkish Seismic Code, which came into force on January 1st, 2019 specifies four different levels of earthquake ground motion:

- DD-1: 2% probability of exceeding in 50 years, corresponding to a return period of 2475 years.
- DD-2: 10% probability of exceeding in 50 years, corresponding to a return period of 475 years.
- DD-3: 50% probability of exceeding in 50 years, corresponding to a return period of 72 years.
- DD-4: 50% probability of exceeding in 30 years, corresponding to a return period of 43 years.

The 5% damped elastic design spectrum (Fig. 2.9) is defined in terms of design spectral accelerations at the short period (S_{DS}) and the 1 sec. period (S_{D1}). The interactive application provided by the Disaster and Emergency Management Presidency (AFAD) of Turkey can be accessed through the web site https://tdth.afad.gov.tr/. Required parameters to calculate the location-specific elastic design spectrum can be generated via the interactive application by entering the coordinates of the structure and the soil class.

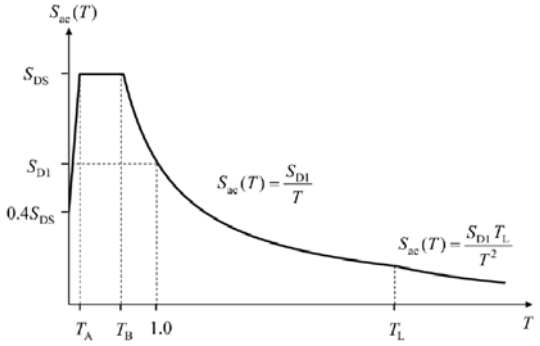

Fig. 3.9 Elastic design spectrum (TSC, 2018).

In the design spectrum, T_A and T_B are the corner periods, which are calculated as given by Eq. (4), and T_L is equal to 6 sec.

$$T_A = 0.2\frac{S_{D1}}{S_{DS}} \qquad T_B = \frac{S_{D1}}{S_{DS}} \tag{4}$$

The response spectrum is constructed using the equations below,

$$S_{ae}(T) = \left(0.4 + 0.6\frac{T}{T_A}\right)S_{DS} \qquad (0 \le T \le T_A) \tag{5}$$

$$S_{ae}(T) = S_{DS} \qquad (T_A \le T \le T_B) \tag{6}$$

$$S_{ae}(T) = \frac{S_{D1}}{T} \qquad (T_B \le T \le T_L) \tag{7}$$

$$S_{ae}(T) = \frac{S_{D1}T_L}{T^2} \qquad (T_L \le T) \tag{8}$$

5% damped elastic response spectrum corresponding to Incirli pedestrian bridge is given by Fig. 2.10. The site class is determined as ZD based on the microzonation map provided by the Istanbul Metropolitan Municipality. The microzonation map can be accessed through the website https://depremzemin.ibb.istanbul/calismalarimiz/tamamlanmis-calismalar/istanbul-ili-mikrobolgeleme-projeleri/.

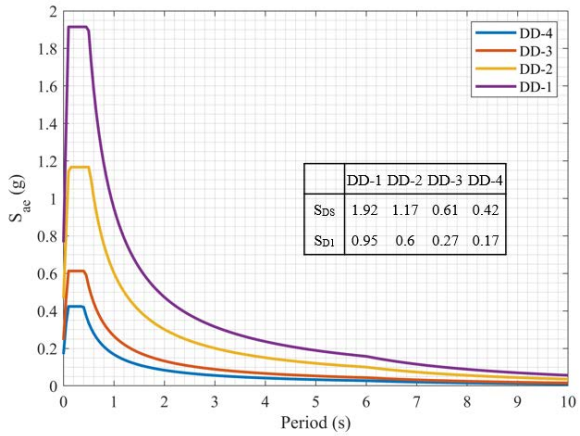

Fig. 3.10 Elastic design spectrum corresponding to Incirli pedestrian bridge.

3.4 EQUIVALENT EARTHQUAKE LOAD ANALYSIS

The equivalent earthquake load is calculated for each level of the earthquake using the elastic spectral acceleration defined in Section 2.2 Code Specified Earthquakes and the total mass of the structure. The total mass of the structure is estimated as 130 t and 135.6 t for the unloaded and fully loaded cases. Base shear and overturning moment resulting in the E-W and N-S directions in the case of unloaded and fully loaded conditions are given by Table 3.

Table 3. Base shear and overturning moment resulting in the E-W and N-S directions in the case of unloaded and fully loaded conditions.

	Unloaded Condition				Fully loaded Condition			
	S_{ae} (g)	M (t)	V_{tE} (kN)	M_o (kNm)	S_{ae} (g)	M (t)	V_{tE} (kN)	M_o (kNm)
DD-1	1.92	130	2442.2	13920.54	1.92	135.6	2547.4	14520.19
DD-2	1.17	130	1488.28	8483.17	1.17	135.6	1552.39	8848.6
DD-3	0.61	130	781.76	4456.03	0.61	135.6	815.43	4647.98
DD-4	0.42	130	540.73	3082.15	0.42	135.6	564.02	3214.91

Calculated base shear and overturning moment are distributed over each column depending on their effective loading area. Base shear and overturning moment corresponding to each element under the effect of the unloaded condition is given by Table 4.

Table 4. Base shear and overturning moment corresponding to each element under the unloaded condition.

Location (m)	DD-1		DD-2		DD-3		DD-4	
	V_{tE} (kN)	M_o (kNm)	V_{tE} (kN)	M_o (kNm)	V_{tE} (kN)	M_o (kNm)	V_{tE} (kN)	M_o (kNm)
0	33.03	188.28	20.13	114.74	10.57	60.27	7.31	41.69
3.1	216.3	1232.93	131.81	751.35	69.24	394.67	47.89	272.98
20.3	219.5	1251.15	133.76	762.45	70.26	400.5	48.6	277.02
23.7	323.92	1846.35	197.4	1125.17	103.69	591.03	71.72	408.8
50.7	404.9	2307.94	246.75	1406.46	129.61	738.78	89.65	511
61.7	397.44	2265.43	242.2	1380.55	127.22	725.17	88	501.59
88	530.63	3024.62	323.37	1843.2	169.86	968.19	117.49	669.68
111.5	283.43	1615.56	172.72	984.52	90.73	517.15	62.75	357.7
114.6	33.03	188.28	20.13	114.74	10.57	60.27	7.31	41.69

Base shear and overturning moment corresponding to each element under the effect of the fully-loaded condition is given by Table 5.

Table 5. Base shear and overturning moment corresponding to each element under the fully loaded condition.

Location (m)	DD-1		DD-2		DD-3		DD-4	
	V_{tE} (kN)	M_o (kNm)	V_{tE} (kN)	M_o (kNm)	V_{tE} (kN)	M_o (kNm)	V_{tE} (kN)	M_o (kNm)
0	34.45	196.39	21.00	119.68	11.03	62.87	7.63	43.48
3.1	225.62	1286.04	137.49	783.71	72.22	411.67	49.95	284.74
20.3	228.95	1305.04	139.53	795.29	73.29	417.75	50.69	288.95
23.7	337.88	1925.89	205.90	1173.64	108.16	616.49	74.81	426.41
50.7	422.34	2407.36	257.38	1467.04	135.19	770.61	93.51	533.01
61.7	414.56	2363.02	252.64	1440.02	132.70	756.41	91.79	523.20
88	553.49	3154.91	337.30	1922.60	177.18	1009.90	122.55	698.53
111.5	295.64	1685.15	180.16	1026.93	94.64	539.42	65.46	373.11
114.6	34.45	196.39	21.00	119.68	11.03	62.87	7.63	43.48

The TSC 2018 suggests determining the horizontal earthquake forces in both major axes separately and combining those forces by taking 100% of the horizontal earthquake forces for one direction and 30% in the perpendicular direction. The bending stresses at the most critical

section of each column in the N-S direction, based on the load combination for bi-directional effects, is presented in Table 6.

Table 6. The bending stress occurs in the N-S direction.

Location (m)	DD-1		DD-2		DD-3		DD-4	
	M_o (KNm)	σ (N/mm^2)	M_o (KNm)	σ (N/mm^2)	M_o (KNm)	σ (N/mm^2)	M_o (KNm)	σ (N/mm^2)
0.00	255.31	40.06	155.58	24.42	81.72	12.82	56.53	8.87
3.10	1671.85	262.36	1018.82	159.88	535.17	83.98	370.16	58.09
20.30	1696.56	266.24	1033.88	162.25	543.08	85.22	375.63	58.95
23.70	2503.66	392.89	1525.73	239.43	801.43	125.77	554.33	86.99
50.70	3129.57	491.12	1907.16	299.29	1001.79	157.21	692.92	108.74
61.70	3071.92	482.07	1872.03	293.77	983.34	154.31	680.15	106.74
88.00	4101.38	643.62	2499.38	392.22	1312.87	206.03	908.09	142.50
111.50	2190.70	343.78	1335.01	209.50	701.25	110.05	485.04	76.12
114.60	255.31	40.06	155.58	24.42	81.72	12.82	56.53	8.87

In the case of DD-3 and DD-4 level earthquakes, none of the column sections reach the yield limit. However, in the case of the DD-1 level earthquake, the bending stress calculated for several columns exceeds the yield stress (335 N/mm^2) of the material. Moreover, in the case of DD-2 level earthquakes, some of the cross-sections will exceed the yield limit.

The bending stress that occurs in the E-W direction, based on the same load combination, is presented in Table 7.

Table 7. The bending stress occurs in the E-W direction.

Location (m)	DD-1		DD-2		DD-3		DD-4	
	M_o (KNm)	σ (N/mm^2)	M_o (KNm)	σ (N/mm^2)	M_o (KNm)	σ (N/mm^2)	M_o (KNm)	σ (N/mm^2)
0.00	255.31	19.63	155.58	11.96	81.72	6.28	56.53	4.35
3.10	1671.85	128.52	1018.82	78.32	535.17	41.14	370.16	28.45
20.30	1696.56	130.42	1033.88	79.48	543.08	41.75	375.63	28.88
23.70	2503.66	192.46	1525.73	117.28	801.43	61.61	554.33	42.61
50.70	3129.57	240.57	1907.16	146.60	1001.79	77.01	692.92	53.27
61.70	3071.92	236.14	1872.03	143.90	983.34	75.59	680.15	52.28
88.00	4101.38	315.28	2499.38	192.13	1312.87	100.92	908.09	69.81
111.50	2190.70	168.40	1335.01	102.62	701.25	53.91	485.04	37.29
114.60	255.31	19.63	155.58	11.96	81.72	6.28	56.53	4.35

None of the columns reach the yield limit for any of the four levels of earthquakes

4 Conclusions

In this report, the seismic risk analysis of Incirli Pedestrian Bridge over D100 Expressway in Istanbul is investigated. Dynamic characteristics of the bridge are identified by performing vibration measurements and field inspection. The transfer matrix formulation of response is used to derive an equivalent SDOF structure for the bridge. The location-specific elastic design spectra are derived based on the latest Turkish seismic design code, TSC2018. Using the identified natural frequency of the structure and the elastic design spectra, the earthquake forces on the bridge for four earthquake levels with different return periods are calculated. The force reduction factor is not used in the calculations (i.e.,R=1). The results show that the structure can resist to all four levels of design earthquakes in the E-W direction. However, in the N-S direction, several columns would yield and undergo plastic deformations under the DD-3 and DD-4 level earthquakes.

References

Çetin, M. (2018): Development of an algorithm and a matlab code for system identification and model calibration of multistory buildings, MSc Thesis, Boğaziçi University, Istanbul, Turkey.

Disaster and Emergency Management Presidency (AFAD) (n.d): Retrieved from https://tdth.afad.gov.tr/TDTH/main.xhtml.

Güralp Systems Limited (n.d): Retrieved from https://www.guralp.com/documents/DAS-050-0006.pdf.

Holzer H (1921): Die berechung der drehscwingungen. Springer, Berlin, Germany.

Istanbul Metropolitan Municipality (IBB) (2007): Retrieved from https://depremzemin.ibb.istanbul/calismalarimiz/tamamlanmis-calismalar/istanbul-ili-mikrobolgeleme-projeleri/.

Kaya, Y., S. Kocakaplan, and E. Şafak (2015): System identification and model calibration of multi-story buildings through estimation of vibration time histories at non-instrumented floors. Bulletin of Earthquake Engineering, 13, no. 11, 3301-3323.

Şafak, E., C. Mueller, and J. Boatwright (1988): A simple model for strong ground motions and response spectra. Earthquake Engineering & Structural Dynamics, 16, no. 2, 203-215.

Thomson W. T. (1993): Theory of Vibration With Applications, NJ, Englewood Cliffs:Prentice-Hall.

TSC 2018 (2018): Turkish Seismic Code 2018. Disaster and Emergency Management, Ankara, Turkey.